

An Energy-Constrained Parameterization of Eddy Buoyancy Flux

PAOLA CESSI

Scripps Institution of Oceanography, University of California, San Diego, La Jolla, California

(Manuscript received 28 March 2007, in final form 18 December 2007)

ABSTRACT

A parameterization for eddy buoyancy fluxes for use in coarse-grid models is developed and tested against eddy-resolving simulations. The development is based on the assumption that the eddies are adiabatic (except near the surface) and the observation that the flux of buoyancy is affected by barotropic, depth-independent eddies. Like the previous parameterizations of Gent and McWilliams (GM) and Visbeck et al. (VMHS), the horizontal flux of a tracer is proportional to the local large-scale horizontal gradient of the tracer through a transfer coefficient assumed to be given by the product of a typical eddy velocity scale and a typical mixing length. The proposed parameterization differs from GM and VMHS in the selection of the eddy velocity scale, which is based on the kinetic energy balance of baroclinic eddies. The three parameterizations are compared to eddy-resolving computations in a variety of forcing configurations and for several sets of parameters. The VMHS and the energy balance parameterizations perform best in the tests considered here.

1. Introduction

Global altimetric observations reveal robust meso-scale eddy activity with maxima in the tropics, the western boundary current extension of the subtropical gyres, and the equatorward side of the Antarctic Circumpolar Current (ACC; Maximenko et al. 2005; Stammer et al. 2006). The typical horizontal scale of the eddies l_e ranges from 80 to about 200 km, decreasing as latitude increases (Stammer 1997). The variation of l_e with latitude is at a rate consistent with the deformation radius dependence $l_e \propto f^{-1}$, although the eddies are systematically larger than the local baroclinic radius.

The scarcity of data precludes global estimates of eddy heat and salt transports; however, the eddy contribution to the heat and tracer transport has been shown to be important in the western boundary current extension, near the equator, and in the ACC, although it is probably negligible in the gyres' interior (Wunsch 1999; Jayne and Marotzke 2002). Although limited in space, the regions where eddy fluxes are important coincide with areas of strong heat flux exchange with the atmosphere, and it is probable that eddy heat fluxes are

crucial in the earth's heat budget. Despite this, the oceanic component of the global climate models is unable to resolve eddy scales, except in computations about a decade long (Maltrud and McClean 2005) and for one set of climate scenarios.

For climate-oriented computations that are integrated for centuries and for several sets of external parameters, typical resolutions are 1° latitude and longitude, so that eddy fluxes of heat and other tracers have to be parameterized in terms of the coarsely resolved variables. These closures usually have at least one undetermined constant that needs to be tuned to either high-resolution numerical simulations or observations. To be useful for climate scenarios or geographical regions other than that used for tuning, a successful eddy flux closure must contain the appropriate parametric dependence. One way to achieve the correct dependence on external parameters is to constrain the eddy flux closures with conservation laws. In this study we use an approximation of the eddy energy balance (EB) as a partial constraint on eddy parameterizations.

2. Parameterization of eddy fluxes

In coarse-grid models a typical tracer variable \bar{C} evolves according to

$$\bar{C}_t + \nabla_h(\bar{\mathbf{v}}\bar{C}) + (\bar{w}\bar{C})_z + \nabla_h(\bar{\mathbf{v}}'\bar{C}') + (\bar{w}'\bar{C}')_z = \overline{\text{Sources}}. \quad (1)$$

Corresponding author address: Paola Cessi, 9500 Gilman Drive, UCSD-0213, La Jolla, CA 92093-0213.
E-mail: pcessi@ucsd.edu

The overbar denotes the mean quantity, which is time averaged over a period longer than the typical eddy turnover time, and the prime symbol denotes the departure from the mean. Because the length scales of the primed quantities are unresolved by a coarse grid, the fluxes induced by the unresolved eddies must be expressed in terms of mean quantities, such as \overline{C} .

a. Skew fluxes

Modern parameterizations of eddy fluxes of tracers take the point of view that the transport occurs largely along rather than across buoyancy surfaces, and they take care to separate this “skew” or advective component from the properly diffusive part, which represents irreversible mixing processes and is usually smaller (e.g., Griffies 1998). In this study we focus on the advective component of the eddy fluxes only. Following Griffies (1998), we express the flux of tracers as

$$\begin{aligned}\overline{\mathbf{v}'C'} &= -\kappa_e \nabla_h \overline{C}, \\ \overline{w'C'} &= -\kappa_e (2\mathbf{S} \cdot \nabla_h \overline{C} + S^2 \overline{C}_z).\end{aligned}\quad (2)$$

We have denoted the eddy diffusivity with κ_e , and $\mathbf{S} \equiv -\nabla_h \overline{b}/\overline{b}_z$ is the horizontal vector whose components are the slopes of the buoyancy surfaces.

When the tracer is buoyancy itself, it is clear that the eddy flux thus defined is perpendicular to the buoyancy gradient, and is not a “downgradient” diffusivity. With $\kappa_e > 0$, the horizontal component $\overline{\mathbf{v}'b'}$ is against the mean horizontal buoyancy gradient; however, the vertical component is up the vertical buoyancy gradient and is given by

$$\overline{w'b'} = \kappa_e S^2 \overline{b}_z. \quad (3)$$

These properties have been thoroughly discussed in the literature (Griffies 1998), and the main point is that the formulation (2) leaves the buoyancy variance (or entropy) unchanged, as required for advective fluxes.

b. Estimating the eddy “diffusivity” κ_e

The formulation (2) requires the specification of the eddy diffusivity κ_e , which can be a function of time and space. The simplest choice is $\kappa_e = \kappa_{\text{GM}}$, with κ_{GM} being constant. This is the choice of Gent and McWilliams (1990, hereafter GM90; see also Gent et al. 1995).

Another approach is to equate κ_e to a typical eddy velocity v_e times a typical mixing length l_e . Within this framework, Visbeck et al. (1997, hereafter VMHS), following Green (1970) and Stone (1972), determine v_e and l_e based on the insight offered by the linear stability analysis of a constant baroclinic shear with a background constant stratification in a zonally reentrant geometry. Thus, VMHS select $v_e = l_e/t_e$, with

$t_e^{-1} = H|\nabla \overline{b}|/(fl_R)$ (where $l_R = \sqrt{|\overline{b}_z|H}/f$ is the deformation radius), where H is the domain’s depth, and f is the rotation rate. The rationale for this choice comes from Eady’s linear stability analysis (Eady 1949), which identifies the Rossby deformation radius l_R as the fastest-growing scale, with growth rate t_e^{-1} . In terms of v_e , VMHS’s choice coincides with that proposed by Larichev and Held (1995) using scaling arguments for geostrophic turbulence based on equipartition of eddy kinetic and eddy available potential energy. The equipartition assumption, together with the assumption that the baroclinic eddy velocity scales as the mean baroclinic velocity, leads to estimation of the barotropic eddy velocity¹ as $v_e = \overline{u}_{\text{bc}} l_e / l_R$, with $\overline{u}_{\text{bc}} = H|\overline{b}_y|/f$, that is, the zonally averaged baroclinic velocity scale. Other assumptions about the eddy velocity spectra lead to different dependences of v_e on the mean shear (cf. Smith and Vallis 2002).

Our approach is similar to VMHS’s, in that we try to separately estimate the typical eddy velocity and mixing length. However, our estimate stems from the analysis of nonlinearly equilibrated eddy fields, rather than the linear growth of disturbance upon a prescribed mean field.

The energy balance analysis, presented in the next section, indicates that in a statistical steady state the conversion of eddy potential energy is balanced by the viscous dissipation of eddy kinetic energy. The viscous removal of eddy kinetic energy is dominated by bottom drag, because the equilibration of the eddy turbulence is subject to an inverse cascade, which favors dissipation at large horizontal scales, and leads to the barotropization of the eddies. This balance determines the typical barotropic eddy velocity scale v_e .

c. A zonally averaged example

An explicit formula is given here for the case where the mean component of the flow is zonally and temporally averaged, and thus varies only in depth z and latitude y . Thus, hereafter an overbar denotes a zonal and temporal average. This configuration, appropriate for a zonally periodic geometry such as the ACC, provides an unequivocal distinction between the mean and fluctuating component, because it involves a separation of horizontal length scales as well as time scales. The derivation is easily generalized to three dimensions, but the parameterization has not been tested in this more general context.

¹ The eddy velocity that needs to be estimated is the barotropic component, because the baroclinic velocity is in thermal wind balance, largely orthogonal to the horizontal buoyancy gradient, and thus is unable to advect buoyancy.

The eddy energy balance (19), derived in the following section, suggests a typical eddy velocity v_e , given by

$$v_e(y) \approx \sqrt{r^{-1}\langle w'b' \rangle}. \quad (4)$$

The angled brackets, defined as

$$\langle \rangle \equiv (LHt_\infty)^{-1} \int_0^{t_\infty} dt \int_{-H}^0 dz \int_0^L dx,$$

indicate a temporal, zonal, and vertical average (L is the longitudinal extent of the domain). The symbol r denotes the spin-down rate resulting from bottom drag. To complete the parameterization we need to specify the mixing length, an issue that is discussed later. The important assumption here is that l_e is independent of z . With this additional restriction we have the relation for the energy balance (EB) diffusivity:

$$\kappa_{\text{EB}} \approx l_e \sqrt{r^{-1}\langle w'b' \rangle}. \quad (5)$$

Using the relation (3) to get an expression for κ_{EB} in terms of the mean quantities, we find

$$\kappa_{\text{EB}} = cl_e^2 \langle \bar{b}_y^2 / \bar{b}_z \rangle / r = \frac{cl_e^2}{rH} \int_{-H}^0 \bar{b}_y^2 / \bar{b}_z dz, \quad (6)$$

where c is a nondimensional constant, which is determined by the procedure described in section 4c. This formula is our proposal for the eddy diffusivity and should be compared with the expression advanced by VMHS (γ is a dimensionless constant):

$$\kappa_{\text{VMHS}} = \gamma l_e^2 f \langle |\bar{b}_y| / \sqrt{\bar{b}_z} \rangle = \frac{\gamma l_e^2 f}{H} \int_{-H}^0 |\bar{b}_y| / \sqrt{\bar{b}_z} dz. \quad (7)$$

The diffusivities κ_{EB} in (6) and κ_{VMHS} in (7) are rather similar in their dependence on the mean buoyancy gradient, but differ in their parametric dependence. Specifically, κ_{EB} depends explicitly on the bottom drag r , while κ_{VMHS} does not. Equivalently, our proposal for the eddy velocity is

$$v_{e\text{EB}} = \frac{l_e \bar{b}_y^2}{r \bar{b}_z},$$

while the eddy velocity proposed by VMHS is

$$v_{e\text{VMHS}} = l_e f \frac{|\bar{b}_y|}{\sqrt{\bar{b}_z}}.$$

There is a quantitative difference of the dependence on the mean temperature gradient, while there is a qualitative difference in the dependence on the frictional parameter r .

Expression (6) is equivalent to the eddy diffusivity found by Thompson and Young (2006) for the eddy diffusivity in a quasigeostrophic two-layer model, as-

suming that the eddies are a dilute gas of vortices.² We also share with Thompson and Young (2006) the inability to offer a scaling for the mixing length l_e . Our numerical simulations are consistent with the notion that l_e increases with decreasing bottom drag (cf. Cessi et al. 2006, their Fig. 6), but we cannot offer a convincing scaling argument to quantify this dependence.

To complete the parameterization it is necessary to specify the mixing length l_e . We have not been able to provide a physical scaling argument that agrees with the results of our numerical simulations. After experimentation, we find that the mixing length can be described by the Wentzel–Kramers–Brillouin (WKB)³ approximation of the Rossby deformation radius, and thus we set

$$l_e = f^{-1} \int_{-H}^0 \sqrt{\bar{b}_z} dz. \quad (8)$$

The scale (8) is also used in our implementation of the VMHS parameterization (7). This choice differs from the “width of the baroclinic zone” used by VMHS, defined as the meridional width over which the Eady linear growth rate $|\bar{b}_y| / \sqrt{|\bar{b}_z|}$ exceeds a fraction (10%) of the maximum linear growth area of the region. Because of the ambiguity of this definition and its nonlocal character, the simpler choice (8) is used here. However, Haine and Marshall (1998) show that, in simulations of a front in a mixed layer, the scale of the front is a better choice than the deformation radius for the mixing length. The goal here is to compare the different choices of velocity scales in parameterizations of baroclinic eddies.

Notice that in the definitions (6) and (7), the eddy diffusivities contain vertically integrated quantities, and are thus independent of z . This choice is supported by diagnostics of the eddy-resolving simulations (see section 4b). The nonlocality in the vertical direction is unavoidable given that the baroclinic life cycle involves the coupling of vertical modes, and in particular the interaction of the barotropic mode with at least one baroclinic mode.

3. Eddy energy balance

In this section the mechanical energy balance for eddies is examined starting from the primitive equations,

² The expression (29) in Thompson and Young (2006) is more complicated than (6) because they consider two layers of equal depth. However, (6) is recovered from their Eq. (29) in the limit of an upper layer that is much thinner than the total depth of the domain.

³ The WKB definition of the Rossby deformation radius differs from (8) by a factor of π . Here, this factor is absorbed in the constants c and γ in (6) and (7).

which is the approximation appropriate for oceanic motions on scales from the baroclinic deformation radius to the planetary scale. The primitive equations system is also the one used for direct numerical simulations. The goal of this section is to justify the choice of eddy velocity scaling (4).

The system is governed by

$$\begin{aligned} \frac{Du}{Dt} - fv + p_x &= \nabla \cdot \nu \nabla u + \delta_s^{-1} \gamma_s \tau_s - r \gamma_b u + \nu_6 \nabla^6 u, \\ \frac{Dv}{Dt} + fu + p_y &= \nabla \cdot \nu \nabla v - r \gamma_b v + \nu_6 \nabla^6 v, \\ p_z &= b, \\ \frac{Db}{Dt} &= \nabla \cdot \kappa \nabla b, \\ \nabla \cdot \mathbf{u} &= 0. \end{aligned} \quad (9)$$

We indicate pressure divided by the constant mean density with p , because this is the dynamical quantity in the Boussinesq approximation. The velocity is $\mathbf{u} = (u, v, w)$ and the vertical coordinate is $-H < z < 0$, where H is the constant depth. The horizontal coordinates are $0 < x < L_x$ and $0 < y < L_y$; b is the buoyancy.

We consider a doubly periodic geometry, where periodicity is imposed in both the latitudinal as well as the longitudinal directions. This configuration avoids boundary effects and is numerically efficient. The Coriolis parameter f is constant.

a. Forcing and dissipation

The momentum equation is forced by a zonal stress concentrated near the surface, located at $z = 0$. This wind stress is modeled as a body force in (9); $\delta_s^{-1} \gamma_s(z) \tau_s(y) \hat{x}$. Here, $\tau_s(y)$ is a specified pattern of wind stress and the constant $\delta_s \ll H$ is the depth of the surface layer. We use a sinusoidal wind profile

$$\tau_s(y) = -\tau \sin(2\pi y/L_y + \phi), \quad (10)$$

where ϕ is the phase of the wind relative to the origin of the domain and $\tau > 0$ is the strength of the wind stress. The nondimensional ‘‘surface function’’

$$\gamma_s(z) \equiv \sqrt{\frac{2}{\pi}} e^{-z^2/2\delta_s^2}, \quad (11)$$

tapers the body force $\tau_s(y)$ smoothly to zero in the ocean interior. We use $\delta_s = 40$ m. The surface function γ_s is normalized so that

$$\int_{-H}^0 \gamma_s(z) dz = \delta_s. \quad (12)$$

This normalization ensures that the total flux of zonal momentum into the water column is $\tau_s(y)$. Distributing

the wind stress over a ‘‘surface forced layer’’ with specified thickness δ_s relieves the model from resolving Ekman layers.

The bottom stress divergence is also represented as a body force $-r \gamma_b(z)(u \hat{x} + v \hat{y})$ in (9). This bottom drag force is applied over a layer of thickness $\delta_b \ll H$ using the bottom-concentrated function

$$\gamma_b(z) \equiv \frac{H}{\delta_b} \sqrt{\frac{2}{\pi}} e^{-(z+H)^2/2\delta_b^2}, \quad (13)$$

which is chosen to have a unit vertical average. We use $\delta_b = 40$ m. The time scale r^{-1} controls the strength of the bottom drag and is the spin-down time of the barotropic velocities.

b. Small-scale mixing

The eddy diffusivities $\nu(z)$ and $\kappa(z)$ represent small-scale mixing processes, such as breaking internal gravity waves and mixed layer turbulence. As a simple model of enhanced diffusivity in the surface layer we use

$$\kappa(z) = \kappa_a + \kappa_s \gamma_s(z), \quad (14)$$

where $\gamma_s(z)$ is the Gaussian surface function in (11); here, $\kappa(z)$ represents small-scale mixing processes, such as breaking internal gravity waves and mixed layer turbulence. The constant κ_a is the small ‘‘abyssal’’ diffusivity, and κ_s is the surface diffusivity that maintains the mixed layer. For the viscosity we take $\nu(z) = P\kappa(z)$, where the constant P is a Prandtl number. The debatable choice of a constant Prandtl number presumes that the mixing of momentum and tracers is enhanced at the same rate in the mixed layer: this choice ensures that there is only one externally imposed depth scale.

Because the stresses are modeled as interior sources and sinks, the top and bottom boundary conditions are $\nu u_z = \nu v_z = 0$. In this way, the primary source of mechanical energy dissipation is the bottom drag, rather than Newtonian friction.

c. Buoyancy forcing

The thermal forcing at the surface $z = 0$ is applied with a fixed buoyancy boundary condition

$$b(x, y, 0, t) = b_s(y), \quad (15)$$

and again we use the sinusoidal profile

$$b_s(y) = -B \cos(2\pi y/L_y); \quad (16)$$

B is a positive constant.

Some earlier idealized studies (Karsten et al. 2002; Kuo et al. 2005) impose the buoyancy flux over part of the ocean surface. This fixed-flux limit is certainly ap-

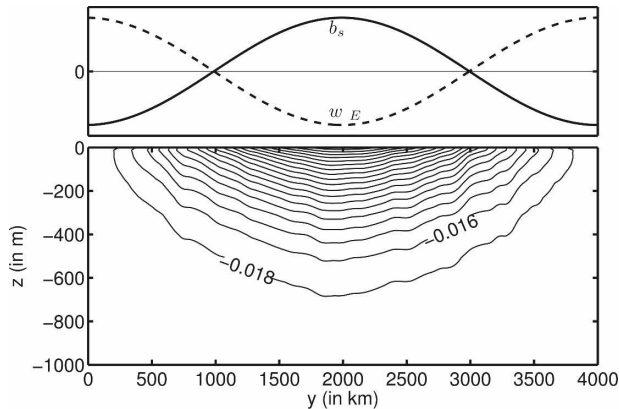


FIG. 1. (bottom) The zonally and temporally averaged buoyancy \bar{b} for run 1 in Table 1 is contoured as a function of z and y (the contour interval is 0.002 m s^{-2}). (top) The surface distribution of buoyancy $b_s(y)$ and the Ekman pumping $w_E(y) = -f^{-1}\tau_{xy}$ is shown. For this set of parameters the buoyancy transport by the zonally averaged flow largely cancels the eddy buoyancy transport.

appropriate when the buoyancy is determined by the salinity, but not heat. For temperature, relaxation to an “apparent atmospheric temperature” approximates the air–sea heat exchange (Haney 1971), with a relaxation time given by $t_{\text{rel}} = \Delta z C_p \rho / \lambda$, where Δz is the depth of the layer over which the relaxation is applied, λ ($\text{W m}^{-2} \text{K}^{-1}$) is the bulk transfer coefficient of heat, C_p is the specific heat, and ρ is the density of water. Using the typical values of $\lambda = 40 \text{ W m}^{-2} \text{K}^{-1}$ and $\Delta z = 7 \text{ m}$ (the depth of the upper layer), we find $t_{\text{rel}} = 7 \times 10^5 \text{ s}$, that is, 8 days. This time scale is shorter than a typical eddy turnover time, estimated at 13 days using an eddy velocity of 0.1 m s^{-1} and an eddy size of 150 km (i.e., average values in our computations). The mean advection times are even larger, so the rapid relaxation to a prescribed temperature can be approximated with the prescription of the surface temperature value, and this is the limit that we consider. Furthermore, using the values just cited, Cessi et al. (2006) show that the eddy statistics are the same when the fixed surface value is replaced with relaxation to an imposed value. The bottom boundary condition has no flux, and $\kappa b_z(x, y, -H, t) = 0$.

d. Three examples of flow

The zonally averaged buoyancy field for three typical eddy-resolving runs is shown in Figs. 1–3. Depending on the phase, ϕ in (10), between the Ekman pumping w_E , induced by the surface wind stress, and the surface buoyancy b_s in (16), the thermocline can be determined by competition between the eddy and mean buoyancy transports (Fig. 1), or by a balance between Ekman

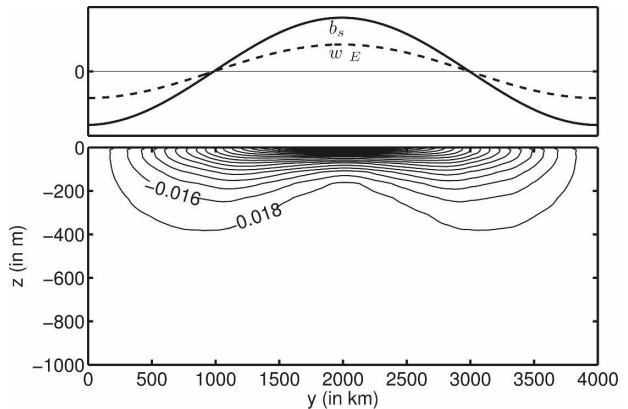


FIG. 2. Same as Fig. 1, but for run 10 in Table 1. For this set of parameters the eddy transport of heat is negligible and the buoyancy transport by the zonally averaged flow is balanced by buoyancy diffusion.

suction and diffusion, á la Munk (1966; Fig. 2). In the former case, the mean circulation is thermally indirect, and the eddies extract the potential energy put into the fluid by the Ekman pumping, which tends to overturn the isopycnals (Gill et al. 1974). The eddies are responsible for restratifying the fluid, and diffusion is unimportant in most of the thermocline; this is the configuration most relevant to the ACC, and its dynamics have been discussed in a number of studies (Karsten et al. 2002; Marshall et al. 2002; Marshall and Radko 2003; Gallego et al. 2004; Kuo et al. 2005; Henning and Vallis 2005; Cessi et al. 2006).

In the second case (Fig. 2), the mean circulation is thermally direct, and the thermocline is a diffusive boundary layer where eddies are largely suppressed;

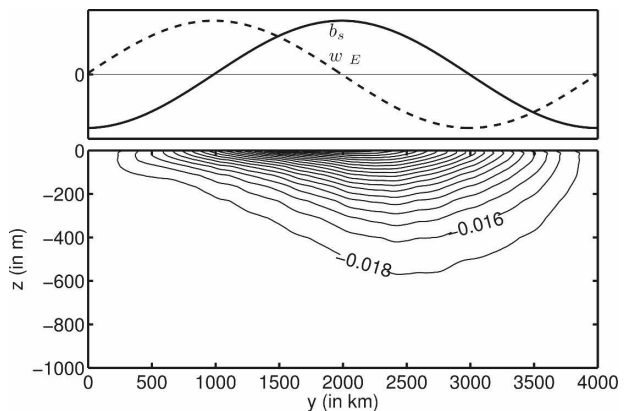


FIG. 3. Same as Fig. 1, but for run 11 in Table 1. For this set of parameters the eddy transport of heat is negligible in the region $0 < y < 2000 \text{ km}$, where the thermocline is thin, and there is Ekman suction, but eddy buoyancy transport is important in the other half of the domain.

Ekman suction flattens the isopycnals, removing available potential energy, and eddies cannot develop.

In Fig. 3 the Ekman pumping is in quadrature with the surface buoyancy, $\phi = -\pi/2$ in (10). This case displays both of the regimes described above: eddies develop preferentially in the downwelling region, leading to a deep thermocline; in the Ekman upwelling region eddies are suppressed, diffusion is important, and the thermocline is thin.

As detailed in Cessi (2007), the relative geometry of surface buoyancy and wind stress curl determines whether potential energy is available to the eddies, and

whether they participate in the buoyancy balance. Eddy parameterizations of buoyancy flux must regulate the strength of the eddies according to the potential energy available in the region of interest, and thus we turn to the eddy energy budget to get scalings for the eddy flux of buoyancy.

e. The eddy energy budget

Dotting \mathbf{v}' into the eddy momentum equations and averaging over time, longitude, and height gives the eddy kinetic energy budget

$$\sum_{i=1,2} \sum_{j=2,3} \langle u'_i u'_j \partial_{x_j} \bar{u}_i \rangle + \left\langle \frac{v}{2} |\mathbf{v}'|^2 \right\rangle_y = -\langle v' p' \rangle_y + \langle w' b' \rangle - r \langle \gamma_b |\mathbf{v}'|^2 \rangle - \langle \nu |\mathbf{v}'_z|^2 \rangle + \langle \nu_6 \mathbf{v}' \cdot \nabla^6 \mathbf{v}' \rangle. \quad (17)$$

In the Reynolds' stress terms, we have used the notation $(x_1, x_2, x_3) = (x, y, z)$ and $(u_1, u_2, u_3) = (u, v, w)$. The wind work, which is the ultimate source of energy in this configuration, does not appear in the eddy energy balance (17); it is part of the mean energy balance instead (cf. Cessi et al. 2006). The fundamental forcing term in (17) is the conversion of available potential energy $\langle w' b' \rangle$.

The first term on the left-hand side of (17) is the sum of the Reynolds' stress conversions between the mean and the eddies. The second term is the advection of eddy kinetic energy by the total flow. To the extent that the scale of the eddies is larger than the deformation radius, the Reynolds' conversions and the advection of kinetic energy are negligible compared to $\langle w' b' \rangle$. Thus the terms on the lhs in (17) can be neglected and we obtain the production/dissipation balance

$$-\langle v' p' \rangle_y + \langle w' b' \rangle \approx r \langle \gamma_b |\mathbf{u}'|^2 \rangle + \langle \nu |\mathbf{v}'_z|^2 \rangle - \langle \nu_6 \mathbf{v}' \cdot \nabla^6 \mathbf{v}' \rangle. \quad (18)$$

For nearly geostrophic eddies $f\mathbf{v}' \approx p'_x$, and the leading order contribution to $\langle v' p' \rangle$ vanishes. However, there is a correlation between the ageostrophic velocity and the pressure, so that in principle the pressure work is of the same order as the conversion of eddy available potential energy. We have diagnosed this term in our computations and it is negligible compared to $\langle w' b' \rangle$. Dissipation is usually dominated by bottom drag (the first term on the rhs), with vertical dissipation (the second term on the rhs) and hyperviscosity (the third term on the rhs) being smaller and usually negligible. Thus, we have the eddy energy balance

$$\langle w' b' \rangle \approx r \langle \gamma_b |\mathbf{u}'|^2 \rangle. \quad (19)$$

The relation (19) is used to scale the typical barotropic eddy velocity in (4). We note that this approximation does not hold for the computations with the lowest values of κ (runs 6 and 9 in Tables 1 and 3), where dissipation by vertical viscosity and hyperviscosity are of the same order or larger than dissipation by bottom drag.

Because γ_b is bottom trapped, only the bottom velocity enters the rhs of (19). In the following we argue that we can estimate the bottom velocity with the barotropic component. We can estimate the error of this approximation by provisionally assuming equipartition of eddy kinetic energy between the baroclinic and barotropic mode.⁴ In all our computations we find that a single vertical scale h characterizes the mean shear, the depth of the thermocline, and the baroclinic eddy velocity (cf. Cessi and Fantini 2004; Cessi et al. 2006). Using this scale and the eddy kinetic energy equipartition hypothesis, we can estimate the surface eddy baroclinic velocity $u'_s u'_s$ through the scaling relation $u'_s \sim u'_B \sqrt{H/h}$ (u'_B is the barotropic eddy velocity and H is the total depth of the domain). Because the baroclinic velocity has a zero depth average, its value at the bottom u'_b must satisfy the approximate relation $(H-h)u'_b + hu'_s \sim 0$. When $h \ll H$, this gives

$$u'_b \sim u'_B \sqrt{h/H}, \quad (20)$$

so that the contribution of the baroclinic component to the bottom velocity is smaller than the barotropic component for $h \ll H$. This scaling is consistent with the

⁴ In the case of small bottom drag geostrophic turbulence theory predicts that the barotropic kinetic energy dominates the baroclinic eddy kinetic energy. Thus, the estimate of the baroclinic velocity obtained assuming equipartition is an upper bound of the actual value.

TABLE 1. The parameter values for the primitive-equation model in the doubly periodic configuration are $H=2000$ m, $L_x = 2 \times 10^6$ m, $L_y = 4 \times 10^6$ m, $f = 10^{-4} \text{ s}^{-1}$, $B = 2 \times 10^{-2} \text{ m s}^{-2}$, $\tau = 1 \times 10^{-4} \text{ m}^2 \text{ s}^{-2}$, and $\nu = 4.5 \times 10^{-4} \text{ m}^2 \text{ s}^{-1}$, $\Delta x = \Delta y = 10.417$ km. The training run is shown in boldface.

Run	$\kappa_a(\text{m}^2 \text{ s}^{-1})$	$\kappa_s(\text{m}^2 \text{ s}^{-1})$	ϕ	$r(\text{s}^{-1})$
1	8×10^{-5}	0	0	2.2×10^{-7}
2	8×10^{-5}	0	0	4.4×10^{-7}
3	8×10^{-5}	0	0	8.9×10^{-7}
4	8×10^{-5}	5.1×10^{-3}	0	2.2×10^{-7}
5	4×10^{-5}	3.1×10^{-3}	0	1.6×10^{-7}
6	2×10^{-5}	1.6×10^{-3}	0	1.1×10^{-7}
7	8×10^{-5}	5.1×10^{-3}	0	4.5×10^{-7}
8	4×10^{-5}	3.1×10^{-3}	0	2.2×10^{-7}
9	2×10^{-5}	1.6×10^{-3}	0	2.2×10^{-7}
10	8×10^{-5}	0	π	2.2×10^{-7}
11	8×10^{-5}	0	$-\pi/2$	2.2×10^{-7}

finding of Thompson and Young (2006) that the bottom velocity cannot be well approximated by the barotropic component in a two-layer model with equal layer depths, despite barotropization of the eddies.

Diagnostics confirm that estimating the bottom velocity with the barotropic component is a good approximation, as long as the thermocline is much thinner than the total depth, consistent with the weak dependence of the baroclinic correction on the small parameter h/H .

4. Comparison with eddy-resolving simulations

a. Method of solution

In this section we test the energy balance parameterization (6), as well as the GM90 and VMHS proposals, against eddy-resolving simulations. The latter are obtained by solving (9) with a finite-difference primitive-equation model in a doubly periodic domain, as described in Cessi and Fantini (2004). The horizontal resolution is 10 km, with a domain size of $L_x \times L_y = 2000 \text{ km} \times 4000 \text{ km}$. The vertical resolution is variable, ranging from 7 m near the top and bottom, in order to resolve the vertical structures of γ_s and γ_b defined in (11) and (13) to 130 m in the center. The total domain depth is $H = 2000$ m.

The parameterizations are applied to the solution of the 2D problem⁵

$$\bar{b}_t + (\bar{v}\bar{b})_y + (\bar{w}\bar{b})_z - (\kappa_e \bar{b}_y)_y + (\kappa_e \bar{b}_y^2 / \bar{b}_z)_z = \nabla \cdot (\kappa \nabla \bar{b}). \quad (21)$$

⁵ Because of the model's coarse resolution, convective adjustment is also employed here, while there is no convective adjustment in the eddy-resolving model.

The mean velocities are calculated by analytically solving the approximate zonal momentum balance

$$\begin{aligned} -f\bar{v} &\approx \delta_s^{-1} \gamma_s(z) \tau_s(y) - r \gamma_b(z) \bar{u}, \\ f\bar{u} + \bar{p}_y &\approx 0, \\ \bar{p}_z &= \bar{b}, \\ \bar{v}_y + \bar{w}_z &= 0. \end{aligned} \quad (22)$$

The zonal flow \bar{u} is obtained using the thermal wind balance $f\bar{u}_z = -\bar{b}_y$, with the barotropic component constrained by the depth integral of the zonal momentum equation, that is,

$$r \int_{-H}^0 \gamma_b(z) \bar{u}(y, z) dz = \tau_s(y). \quad (23)$$

Given the definitions (11) and (13), this implies that

$$-f\bar{v} \approx \tau_s(y) [\delta_s^{-1} \gamma_s(z) - H^{-1} \gamma_b(z)]. \quad (24)$$

The vertical velocity \bar{w} can then be obtained from the divergence equation. The comparison with the full numerical solution of \bar{v} shows that (24) is an excellent approximation.

b. The importance of the barotropic mode

Before elaborating on the quantitative comparison between the resolved and parameterized eddies it is useful to verify the assumption that the barotropic eddy velocities are controlling the eddy buoyancy flux. A simple test of this hypothesis compares the eddy flux $\overline{v'b'}$ with $-a\sqrt{\psi_{\text{BT}}'^2 \bar{b}_y}$, where ψ_{BT}' is the barotropic component of the eddy streamfunction, that is,

$$\psi_{\text{BT}}' \equiv \frac{f}{H} \int_{-H}^0 p' dz,$$

where p is the pressure. The nondimensional constant a is fitted by minimizing the least squares error ε defined as

$$\varepsilon = \sum (\overline{v'b'} + a\sqrt{\psi_{\text{BT}}'^2 \bar{b}_y})^2. \quad (25)$$

All quantities are diagnosed from the eddy-resolving computations. The sum in (25) is taken over all the points of the domain in the meridional vertical plane.

Figure 4 shows $\overline{v'b'}$ and $-a\sqrt{\psi_{\text{BT}}'^2 \bar{b}_y}$ for a typical computation. For the example shown in Fig. 4, the normalized rms error is 0.24 (and $a = 0.90$). The normalized rms error is defined as $\sqrt{\varepsilon / \Sigma(\overline{v'b'})^2}$.

This error is substantially less than that obtained by fitting a constant diffusion coefficient to estimate the flux, as in GM90; the normalized rms error between $\overline{v'b'}$ and $-\kappa_{\text{GM}} \bar{b}_y$ is 0.49.

A related estimate of the eddy flux has been ad-

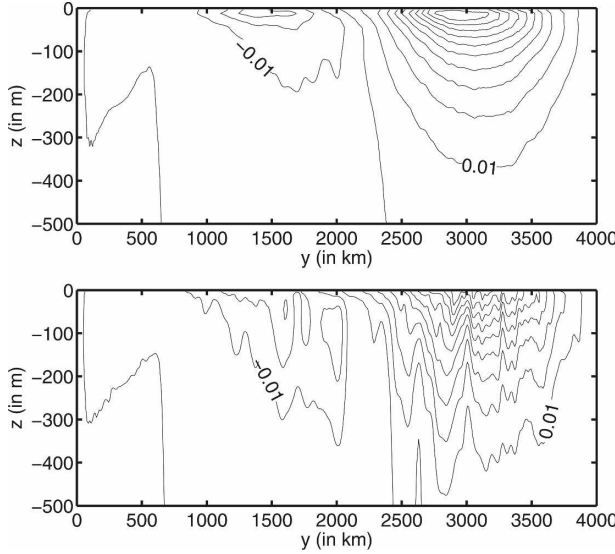


FIG. 4. (top) The quantity $\overline{v'b'}$ in the top 500 m for the eddy-resolving computation 11 in Table 1. The corresponding distributions of Ekman pumping and surface buoyancy are shown in Fig. 3. (bottom) The quantity $-a\sqrt{\psi_{\text{BT}}^2 \bar{b}_y}$, diagnosed for the same computation and using the same contour level. The constant a is determined by minimizing the least squares error between $\overline{v'b'}$ and $-a\sqrt{\psi_{\text{BT}}^2 \bar{b}_y}$. The normalized rms error between the two fields is 0.24, and $a = 0.90$.

vanced by Holloway (1986) using the rms surface streamfunction ψ'_s , instead of the barotropic streamfunction. Holloway's is an attractive proposal because the surface streamfunction is much easier to estimate from observations than the barotropic streamfunction. Unfortunately, $\sqrt{\psi'_s{}^2}$ is not a good estimate of the eddy diffusivity (cf. Table 2).

A summary of the normalized errors between the three estimates of diffusivity described in this subsection is given in Table 2. The barotropic eddy streamfunction is a better estimate than a constant diffusivity, and both are better than the surface eddy streamfunction, supporting the choice of estimating the eddy diffusivity with the typical velocity and length scale of the barotropic eddies. In other words, the typical eddy velocity v_e and mixing length l_e should satisfy

$$v_e l_e \propto \sqrt{\psi_{\text{BT}}^2}. \quad (26)$$

c. Quantitative testing of the parameterizations

The procedure adopted to test the parameterizations is as follows. First, the nondimensional constants c in (6), γ in (7), and κ_{GM} are determined by fitting the square of the vertically integrated buoyancy eddy flux, defined as

$$F(y) \equiv \int_H^0 (\kappa_e \bar{b}_y)^2 dz, \quad (27)$$

to the resolved one

$$F_r \equiv H \langle (v'b')^2 \rangle, \quad (28)$$

where the subscript r refers to the resolved computations. We find that this diagnostic is sensitive to both the spatial distribution and the amplitude of the eddy fluxes. The fit is obtained for one "training" simulation and the comparison is then performed for simulations with different sets of parameters, keeping the constants c , γ , and κ_{GM} fixed.

Specifically c , γ , and κ_{GM} are chosen by minimizing the normalized rms error between F and F_r , defined as

$$E_{F,F_r} \equiv \sqrt{\frac{\sum_k [F(y_k) - F_r(y_k)]^2}{\sum_k F_r(y_k)^2}}. \quad (29)$$

The sum in (29) is taken over the points of the low-resolution parameterized computation, which are much fewer than those in the eddy-resolving computation. This procedure gives $c = 1.48$, $\kappa_{\text{GM}} = 7000 \text{ m}^2 \text{ s}^{-1}$, and $\gamma = 7.7$. The value of γ differs from that found by VMHS because we use the definition (8) for the deformation radius rather than the definition for the Eady problem with constant stratification. The two definitions differ by the factor H/h , where H is the domain height and h is the depth of the thermocline; this represents a considerable quantitative difference. Furthermore, as noted in section 2c, our choice of the mixing length differs from that originally adopted by VMHS.

One eddy-resolving computation (run 7 in Table 1) is used to "train" the eddy diffusivity for all three parameterizations. With this choice, $E_{F,F_r} = 0.08, 0.012, 0.31$ for the EB, VMHS, and GM90 parameterizations, respectively. The spatial structure of F is shown in Fig. 5; while the EB and VMHS parameterized fluxes adhere closely to the resolved eddy fluxes, it is not possible to reduce the error of the GM90 parameterization below the level shown. This is because the shape of the GM90 parameterized fluxes is different from that of the resolved one.

Two measures are used to test the performance of the different parameterizations: one is E_{F,F_r} , defined in (29), and the other is the error in the zonally averaged surface flux E_{Q,Q_r} , defined as

$$E_{Q,Q_r} \equiv \sqrt{\frac{\sum_k [Q(y_k) - Q_r(y_k)]^2}{\sum_k Q_r(y_k)^2}}, \quad (30)$$

where $Q(y) = \kappa_0 \bar{b}_{z=0}$ is the buoyancy flux at the surface and $z = 0$ (the subscript r indicates the resolved computation). These two measures are more sensitive than

TABLE 2. The coefficient a , minimizing the least squares error between $\overline{v'b'}$ and $-a \sqrt{\psi_{BT}^2} \overline{b}_y$, is tabulated for the computations in Table 1. The rms errors between $\overline{v'b'}$ and $-a \sqrt{\psi_{BT}^2} \overline{b}_y$, between $\overline{v'b'}$ and $-\kappa_{GM} \overline{b}_y$, and between $\overline{v'b'}$ and $-d \sqrt{\psi_s^2} \overline{b}_y$, are also tabulated (ψ_s is the surface streamfunction, proportional to the surface pressure through f). The coefficients κ_{GM} and d are computed by a least-squares error fit.

Run	a	Rms ($\overline{v'b'}$, $-a \sqrt{\psi_{BT}^2} \overline{b}_y$)	Rms ($\overline{v'b'}$, $-\kappa_{GM} \overline{b}_y$)	Rms ($\overline{v'b'}$, $-d \sqrt{\psi_s^2} \overline{b}_y$)
1	0.70	0.40	0.46	0.62
2	0.76	0.36	0.44	0.68
3	0.78	0.38	0.44	0.80
11	0.90	0.24	0.59	0.48

the zonally averaged buoyancy, which is another field that could be compared (cf. VMHS).

For the training computation (run 7 in Table 1), the error in the surface flux is substantially larger than the error in E_{F,F_r} ($E_{Q,Q_r} = 0.22, 0.29, 0.51$ for the EB, VMHS, and GM90 parameterizations, respectively). In a statistically steady state, Q is given by the convergence of net buoyancy transport. With this wind stress configuration, there is a large cancellation between the vertically integrated mean and eddy meridional buoyancy transports, and the net buoyancy transport is a small residual. This cancellation, combined with the derivative associated with the convergence, leads to a noisier field than the eddy fluxes, and thus to larger errors for the surface flux. To illustrate the local performance of the parameterizations, Fig. 6 compares the surface flux $Q(y)$ of the parameterized computations to the resolved computation.

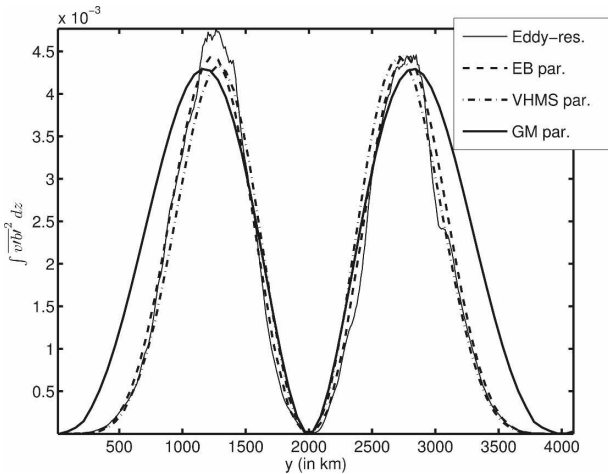


FIG. 5. The square of vertically integrated eddy buoyancy fluxes for the parameterized computations compared with the same quantity for an eddy-resolving computation (thin solid line) for the training set of parameters (run 7 in Table 1). The constants c in (6), γ in (7), and κ_{GM} are determined by minimizing the rms errors (29) between the parameterized and resolved computations (they are 0.08, 0.12, and 0.31 for the EB, VMHS, and GM90 parameterizations, respectively). No value of κ_{GM} reduces the error further.

Figure 7 compares F to F_r for a computation where only the bottom drag is reduced from the training run (run 4 in Table 1). The increase in eddy buoyancy flux above that found in the training run is intermediate between that predicted by the energy balance parameterization and that of the GM90 and VMHS parameterization (which assume no dependence on r). For this computation, the GM90 and VMHS parameterizations perform better than the EB parameterization. This is somewhat surprising, given that the eddy mixing length l_e actually increases as the drag r decreases (cf. Cessi et al. 2006, their Fig. 6), and this dependence, not included in the EB parameterization, would further increase the dependence of the fluxes on r .

Thus, the reasons for failure must be attributed to the breakdown of one or more of the approximations used to derive (6). Diagnostics show that equating the barotropic eddy velocity to the bottom velocity is not a good approximation in those computations with a relatively

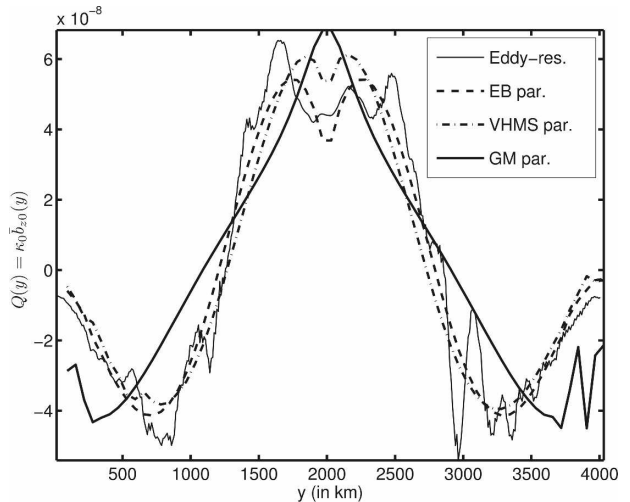


FIG. 6. The net surface flux $Q = \kappa_0 \overline{b}_{z_0}$ for the parameterized computations compared with the same quantity for an eddy-resolving computation (thin solid line) for the training set of parameters (run 7 in Table 1). The least rms errors (30) are given by 0.22, 0.29, and 0.51 for the EB, VMHS, and GM90 parameterizations, respectively.

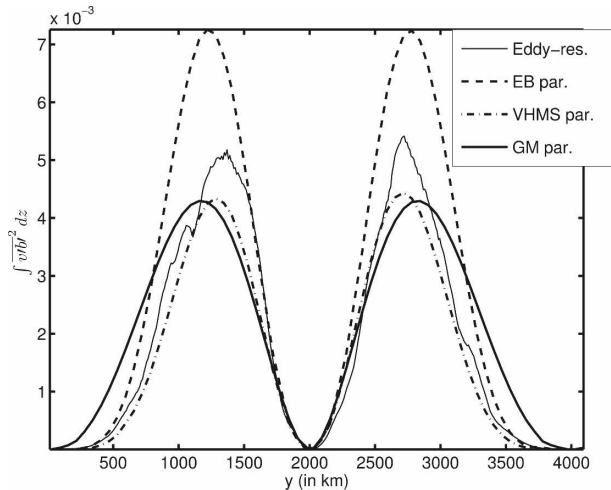


FIG. 7. The square of vertically integrated eddy buoyancy fluxes for the parameterized computations compared with the same quantity for an eddy-resolving computation (thin solid line). The values of the parameters are given in the entry for run 4 in Table 1. Because only the bottom drag r is changed from the values used in run 7, the VMHS and GM90 fluxes are the same as those in Fig. 5.

thick thermocline. In particular, the bottom velocity underestimates the barotropic velocity, and more so for a larger bottom drag. Because the thickness of the thermocline is controlled by the bottom drag (Cessi et al. 2006) the accuracy of the approximation depends on r through the parameter h/H (h is the depth of the thermocline and H is the total depth of the domain). As h/H gets smaller, the approximation gets better. We note that in our calculations $H = 2000$ m, which is a rather shallow depth compared to most large-scale basins, so that it is difficult to have small h/H .

Figure 8 compares F to F_r for the three parameterizations in a case where the wind stress curl is in quadrature with the buoyancy forcing, that is, $\phi = -\pi/2$ in (10); this is run 11 in Table 1. The eddy-resolving zonally averaged buoyancy for this configuration is shown in Fig. 3. In the first half of the domain, $0 \leq y \leq 2000$, the wind generates Ekman suction, which suppresses the generation of eddies. As discussed in more detail in Cessi (2007), the combination of Ekman suction and heating is a sink of eddy available potential energy. Both the VMHS and the EB parameterizations are able to capture the suppression of eddy fluxes in this region, more so than the GM90 parameterization.

Figure 9 shows the resolved and parameterized eddy fluxes in a case where the wind stress curl is in antiphase with the buoyancy forcing, that is, $\phi = \pi$ in (10); this is run 10 in Table 1. The zonally averaged buoyancy for this configuration is shown in Fig. 2. The Ekman upwelling suppresses the generation of eddies in the

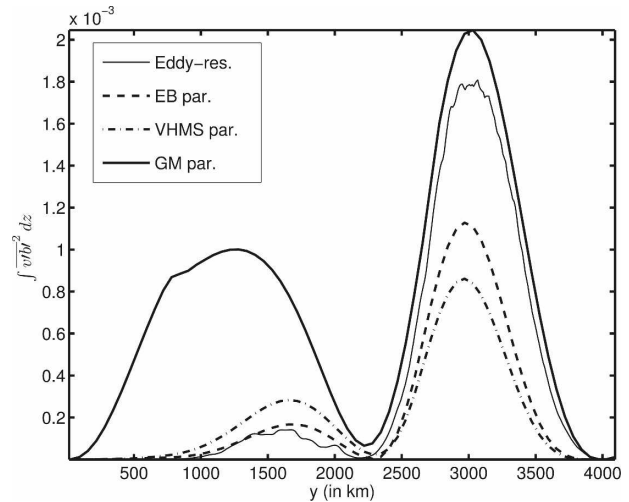


FIG. 8. The square of vertically integrated eddy buoyancy fluxes for the parameterized computations compared with the same quantity for an eddy-resolving computation (thin solid line) for a wind stress in quadrature with the buoyancy forcing, that is, $\phi = -\pi/2$ in (10). The values of the parameter are given in the entry for run 11 in Table 1. The normalized rms errors (29) are $E_{F_{EB}}, F_r = 0.34$, $E_{F_{VMHS}}, F_r = 0.51$, and $E_{F_{GM}}, F_r = 0.90$.

center of the domain and this is well captured by both the VMHS and EB parameterizations, but not by the GM90 parameterization. Despite the large errors in the eddy flux, the net surface flux, which is mostly controlled by the mean circulation, is very well reproduced by both the VMHS and EB parameterizations, and has

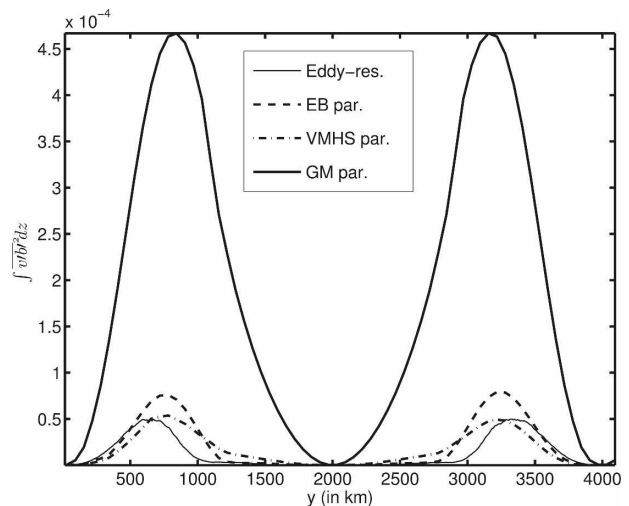


FIG. 9. The square of vertically integrated eddy buoyancy fluxes for the parameterized computations compared with the same quantity for an eddy-resolving computation (thin solid line). The wind stress is in antiphase with the buoyancy forcing, that is, $\phi = \pi$ in (10). The values of the parameters are given in the entry for run 10 in Table 1. The normalized rms errors (29) are $E_{F_{EB}}, F_r = 0.37$, $E_{F_{VMHS}}, F_r = 0.52$, and $E_{F_{GM}}, F_r = 7.20$.

TABLE 3. The errors between the resolved and parameterized fluxes for three parameterizations are tabulated for a subset of the computations in Table 1. The errors in the square of vertically integrated eddy fluxes E_{F,F_r} , are defined in (29) and those in the surface buoyancy fluxes E_{Q,Q_r} , are defined in (30). The training run is shown in boldface. The errors are plotted in Fig. 10.

Run	E_{F,F_r}	E_{F,F_r}	E_{F,F_r}	E_{Q,Q_r}	E_{Q,Q_r}	E_{Q,Q_r}
	EB	VMHS	GM90	EB	VMHS	GM90
1	0.27	0.24	0.31	0.32	0.35	0.30
2	0.19	0.19	0.77	0.30	0.28	0.34
3	0.21	0.33	1.07	0.27	0.28	0.59
4	0.46	0.17	0.28	0.37	0.32	0.43
5	0.27	0.32	0.24	0.25	0.33	0.41
6	0.93	0.20	0.74	0.53	0.34	0.42
7	0.07	0.12	0.31	0.22	0.29	0.51
8	0.14	0.25	0.28	0.18	0.28	0.45
9	0.44	0.23	1.24	0.37	0.30	0.73
10	0.37	0.52	7.20	0.23	0.25	0.35
11	0.34	0.51	0.90	0.27	0.31	0.44

a relatively small error with the GM90 parameterization (cf. run 10 in Table 3).

The performance of all three parameterizations is summarized in Fig. 10, where the rms error for the eddy fluxes E_{F,F_r} and net surface flux of buoyancy E_{Q,Q_r} are plotted as a function of the run number. Because there is an outlier in E_{F,F_r} (GM90 parameterization for run 10), this datum is excluded from the plot. Overall, the largest errors are given by the GM90 parameterization (circles), while the VMHS (squares) and EB (stars) parameterizations have comparable overall performances, with errors around 30%. The largest errors of the EB parameterization are found for run 6, which has the lowest diffusivity and bottom drag. For this computation (and, to a lesser degree, for run 9) the dominant form of energy dissipation is not bottom drag, but vertical viscosity concentrated in the surface mixed layer. Furthermore, even hyperviscosity is larger than the bottom drag, indicating that the energy-containing eddies are poorly resolved. In this regime the approximation (19) to the eddy energy balance fails.

5. Discussion

In this work we developed a parameterization of eddy fluxes built around a constraint from the eddy energy balance. Diagnostics from the direct numerical simulations show that the eddy diffusivity is very well approximated by the rms eddy barotropic streamfunction, and thus is essentially independent of depth. This diagnostic confirms the hypothesis that the barotropic eddy velocity determines the eddy diffusivity, with the baroclinic component affecting a negligible eddy buoyancy flux transport. For nearly geostrophic eddies, the

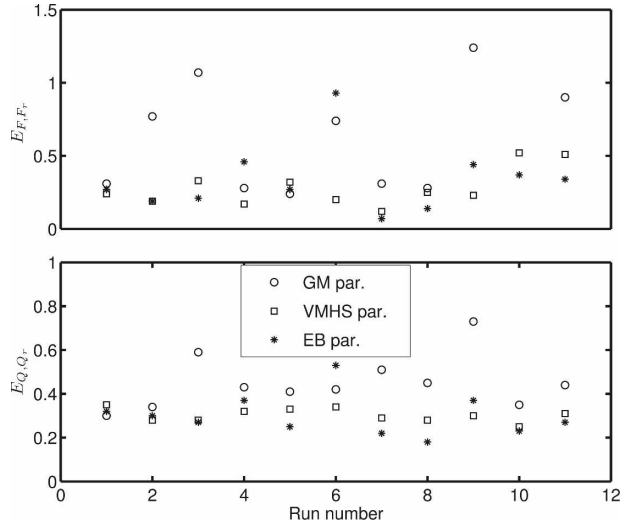


FIG. 10. (top) The normalized rms errors between the parameterized and resolved eddy buoyancy fluxes E_{F,F_r} , defined in (29), excluding the errors of the GM90 parameterization for run 10 in Table 1 (cf. Fig. 9 and Table 3), which would be well outside the plotted range. (bottom) The normalized rms errors between the parameterized and resolved net surface fluxes E_{Q,Q_r} , defined in (30).

buoyancy gradient is largely orthogonal to the baroclinic component of the eddy velocity, which is in thermal wind balance. This result is exact in a two-layer system and holds very well in systems with many vertical modes, as demonstrated by Smith and Vallis (2002).

We estimate the eddy barotropic streamfunction with the barotropic eddy velocity times an eddy mixing length. The barotropic eddy velocity can be approximated with the bottom eddy velocity, which in turn can be obtained by an approximation to the eddy energy balance, (19). The energy balance immediately introduces the bottom drag r as one of the controlling parameters of the eddy diffusivity. This result is consistent with the findings of Thompson and Young (2006) in the context of a quasigeostrophic model.

The velocity estimate needs to be supplemented by an eddy length estimate in order to be used for evaluating the streamfunction. Lacking any explicit constraint on the mixing length, l_e is estimated from eddy-resolving simulations. Assumptions used in the literature, such as the equipartition of eddy kinetic and potential energy (Larichev and Held 1995), are not supported by direct numerical computations (Cessi et al. 2006; Thompson and Young 2006) and cannot be used to predict the mixing length. The optimal fit for l_e indicates an explicit inverse dependence on the bottom drag (Cessi et al. 2006), as found by several studies of geostrophic turbulence on the f plane (Larichev and

Held 1995; Smith et al. 2002; Thompson and Young 2006). However, using the optimally fitted mixing length leads to a worse performance of the parameterization than using the local baroclinic deformation radius (estimated by the WKB approximation). This discrepancy might indicate that the correlation between the eddy velocity and the tracer field depends on more than one length, or, equivalently, that the barotropic eddy streamfunction cannot be estimated by the product of the barotropic eddy velocity times the typical mixing length. This is not surprising given Thompson and Young's (2006) result that the distance between eddies (or vortices) is a length scale that is as important as the typical eddy scale. It is also possible that the poorly resolved loss of balance in the primitive-equation numerical model provides a route for energy dissipation alternative to bottom drag, so that the quasigeostrophic results do not transfer directly to the primitive-equation context.

The new proposal for the eddy flux parameterization is compared to the GM90 scheme and a modified VMHS scheme. The latter equates κ_e to a typical eddy velocity and a typical mixing length, which we chose to be the Rossby deformation radius (the choice of mixing length differs from the original VMHS proposal). However, the VMHS and EB parameterizations differ in the choice of v_e . VMHS make the identification $v_e = l_e/t_e$, where l_e is the distance of particle transfer by eddies and t_e^{-1} is the linear instability growth rate, while we equate v_e to the barotropic component of the eddy velocity, which is estimated using the approximate eddy energy balance. The two choices lead to a similar relation of the eddy diffusivity on the mean vertical and horizontal buoyancy gradient, but differ qualitatively in the dependence on the external parameters, and in particular on the bottom drag.

Despite the uncertainties in the mixing length estimate, both the EB and VMHS parameterizations perform well in comparisons with eddy-resolving simulations where the external parameters are changed, indicating the necessity of including the dependence of κ_e on the local buoyancy gradients, which is absent in the GM90 scheme. Both the VMHS and EB parameterizations involve vertical integrals of mean quantities, but this nonlocality is unavoidable in the equilibration of baroclinic instability, which requires the coupling of at least two vertical modes. In the configuration considered here, we also find that assuming κ_e independent of depth is an excellent approximation.

The dependence of the parameterization on the bottom drag is tested with eddy-resolving simulations in a periodic domain that approximates the ACC geometry.

The dependence on other parameters, such as the rotation rate f , the imposed external buoyancy gradient, and the domain size, has not been tested because of the computational demand of a primitive-equation eddy-resolving model. Although there is a dependence on the bottom drag in the direct numerical simulations, it is not as strong as that predicted by the energy balance parameterization. The reason for this failure is twofold. First, in the regime of weak bottom drag, dissipation is dominated by vertical viscosity, and this prevents estimation of the barotropic velocity component from the eddy energy balance. Second, the approximation that equates the bottom eddy velocity with the barotropic component breaks down when the contribution of the baroclinic component to the bottom velocity becomes comparable to that of the barotropic component. The ratio of the two components depends on r through the following two mechanisms: 1) the ratio of barotropic to baroclinic eddy kinetic energy decreases as r increases because bottom drag primarily affects the barotropic component; and 2) if the eddy kinetic energy were equipartitioned between baroclinic and barotropic modes, the ratio of the corresponding velocities would scale as $\sqrt{h/H}$, that is, the ratio of the thermocline depth to the domain depth. As Cessi et al. (2006) show, h increases with increasing bottom drag, so that the approximation becomes poorer for larger r , or for shallow domains. The net result is that as r becomes larger the approximation becomes less accurate.

In contexts that are more complex than those considered here, other mechanisms might intervene that preclude the simple estimation of the barotropic eddy velocity through the energy balance. One likely suspect is bottom relief. Although the influence of topography on the wind-driven circulation has not been thoroughly examined for the primitive equations, some inferences might be drawn from the quasigeostrophic results. Treguier and Hua (1988) show that while for freely decaying turbulence topography mediates a direct transfer of energy from the barotropic to the baroclinic mode, for turbulence forced by large-scale winds, topography merely slows down the inverse cascade of the barotropic mode. As a result, the eddies become more surface intensified, and this might or might not lead to a breakdown of the approximations as discussed above, depending on whether h becomes smaller or larger.

Finally, the approximate energy balance used to derive the proposed parameterization requires that the Reynolds stress contributions to the energy fluxes be neglected. This is probably not a good approximation in regions where the eddies are organized in jets, such as the mid- and low latitudes.

Acknowledgments. This research was supported by the Office of Science (BER) U.S. Department of Energy, Grant DE-FG02-01ER63252. We acknowledge the National Center for Computational Sciences (NCCS) at Oak Ridge National Laboratory for computational resources used in support of this project. Insightful suggestions from John Marshall and another anonymous referee are gratefully acknowledged.

REFERENCES

- Cessi, P., 2007: Regimes of thermocline scaling: The interaction of wind stress and surface buoyancy. *J. Phys. Oceanogr.*, **37**, 2009–2021.
- , and M. Fantini, 2004: The eddy-driven thermocline. *J. Phys. Oceanogr.*, **34**, 2642–2658.
- , W. R. Young, and J. A. Polton, 2006: Control of large-scale heat transport by small-scale mixing. *J. Phys. Oceanogr.*, **36**, 1877–1894.
- Eady, E. T., 1949: Long waves and cyclone waves. *Tellus*, **1**, 33–52.
- Gallego, B., P. Cessi, and J. C. McWilliams, 2004: The Antarctic Circumpolar Current in equilibrium. *J. Phys. Oceanogr.*, **34**, 1571–1587.
- Gent, P., and J. C. McWilliams, 1990: Isopycnal mixing in ocean circulation models. *J. Phys. Oceanogr.*, **20**, 150–155.
- , J. Willerbrand, T. McDougall, and J. McWilliams, 1995: Parameterizing eddy-induced tracer transports in ocean circulation models. *J. Phys. Oceanogr.*, **25**, 463–474.
- Gill, A. E., J. S. A. Green, and A. J. Simmons, 1974: Energy partition in the large-scale ocean circulation and the production of mid-ocean eddies. *Deep-Sea Res.*, **21**, 499–528.
- Green, J., 1970: Transfer properties of the large-scale eddies in the general circulation of the atmosphere. *Quart. J. Roy. Meteor. Soc.*, **96**, 157–185.
- Griffies, S. M., 1998: The Gent–McWilliams skew flux. *J. Phys. Oceanogr.*, **28**, 831–841.
- Haine, T. W. N., and J. Marshall, 1998: Gravitational, symmetric and baroclinic instability of the ocean mixed layer. *J. Phys. Oceanogr.*, **28**, 634–658.
- Haney, R. L., 1971: Surface thermal boundary condition for ocean circulation models. *J. Phys. Oceanogr.*, **1**, 241–248.
- Henning, C. C., and G. K. Vallis, 2005: The effects of mesoscale eddies on the stratification and transport of an ocean with a circumpolar channel. *J. Phys. Oceanogr.*, **35**, 880–896.
- Holloway, G., 1986: Estimation of oceanic eddy transports from satellite altimetry. *Nature*, **323**, 243–244.
- Jayne, S. R., and J. Marotzke, 2002: The oceanic eddy heat transport. *J. Phys. Oceanogr.*, **32**, 3328–3345.
- Karsten, R., H. Jones, and J. Marshall, 2002: The role of eddy transfer in setting the stratification and transport of a circumpolar current. *J. Phys. Oceanogr.*, **32**, 39–54.
- Kuo, A., A. Plumb, and J. Marshall, 2005: Transformed Eulerian-mean theory. Part II: Potential vorticity homogenization, and the equilibrium of a wind- and buoyancy-driven zonal flow. *J. Phys. Oceanogr.*, **35**, 175–187.
- Larichev, V. D., and I. M. Held, 1995: Eddy amplitudes and fluxes in a homogeneous model of fully developed baroclinic instability. *J. Phys. Oceanogr.*, **25**, 2285–2297.
- Maltrud, M. E., and J. L. McClean, 2005: An eddy resolving global 1/10° ocean simulation. *Ocean Modell.*, **8**, 31–54.
- Marshall, J., and T. Radko, 2003: Residual-mean solutions for the Antarctic Circumpolar Current and its associated overturning circulation. *J. Phys. Oceanogr.*, **33**, 2341–2354.
- , H. Jones, R. H. Karsten, and R. Wardle, 2002: Can eddies set ocean stratification? *J. Phys. Oceanogr.*, **32**, 26–38.
- Maximenko, N. A., B. Bang, and H. Sasaki, 2005: Observational evidence of alternating zonal jets in the world ocean. *Geophys. Res. Lett.*, **32**, L12607, doi:10.1029/2005GL022728.
- Munk, W., 1966: Abyssal recipes. *Deep-Sea Res. J.*, **24**, 1259–1262.
- Smith, K. S., and G. K. Vallis, 2002: The scales of equilibration of mid-ocean eddies: Forced-dissipative flows. *J. Phys. Oceanogr.*, **32**, 1699–1720.
- , G. Boccaletti, C. C. Hennings, I. Marinov, C. Y. Tam, I. M. Held, and G. K. Vallis, 2002: Turbulent diffusion in the geostrophic inverse cascade. *J. Fluid Mech.*, **469**, 13–48.
- Stammer, D., 1997: Global characteristics of ocean variability estimated from regional TOPEX/Poseidon altimeter measurements. *J. Phys. Oceanogr.*, **27**, 1743–1769.
- , C. Wunsch, and K. Ueyoshi, 2006: Temporal changes in ocean eddy transports. *J. Phys. Oceanogr.*, **36**, 543–550.
- Stone, P. H., 1972: A simplified radiative-dynamical model for the static stability of rotating atmospheres. *J. Atmos. Sci.*, **29**, 405–418.
- Thompson, A. F., and W. R. Young, 2006: Scaling baroclinic eddy fluxes: Vortices and energy balance. *J. Phys. Oceanogr.*, **36**, 720–738.
- Treguier, A. M., and B. L. Hua, 1988: Influence of bottom topography on stratified quasi-geostrophic turbulence in the ocean. *Geophys. Astrophys. Fluid Dyn.*, **43**, 265–305.
- Visbeck, M., J. Marshall, T. Haine, and M. A. Spall, 1997: Specification of eddy transfer coefficients in coarse-resolution ocean circulation models. *J. Phys. Oceanogr.*, **27**, 381–402.
- Wunsch, C., 1999: Where do ocean eddy heat fluxes matter? *J. Geophys. Res.*, **104**, 13 235–13 249.